DOI 10.5162/sensoren2024/D5.1

Uncertainty Modeling of a Cyber-Physical Finite Element Sensor Network for Surface Measurements

Lars-Michel Bretthauer[1], Ralf Heynicke[1], Gerd Scholl[1]
[1]Electrical Measurement Engineering, Helmut Schmidt University, Holstenhofweg 85, 22043 Hamburg, Germany

Abstract

In modern manufacturing processes it is mandatory that the components to be manufactured are produced within well-defined manufacturing tolerances. If only small production tolerances are permitted this often means that all production steps have to be monitored, which is a challenging task, e.g. in the production of large-scale components, where it is often not possible to determine the exact shape or surface stress in real-time during forming or deformation processes. Here, a standard solution is the use of laser trackers, typically requiring a human operator or a robot during the measurement process. Also, measurement time increases drastically with the size of the component. In this paper we suggest an approach, where we measure the shape of an object with a finite grid of wireless sensor probes in real-time during the fabrication process. The sensor network measures the surface at discrete points in a similar way classical finite elements (FEM) discretize a volume for modeling the physical behavior. Hence, this measurement system is called a Cyber-Physical Finite-Element-Network (CPFEN). In this paper we present the network structure and the evaluation algorithms that are needed to achieve precise measurements. Also, we model the uncertainty of each local connection and the propagation of uncertainties throughout the network. The “Guide to the expression of uncertainty in measurement“ (GUM) [1] is used for the uncertainty modeling. Thus, it is possible to make a statement about the reliability and accuracy of the complete network.

Keywords: Sensor Network, Inclination Sensor, Uncertainty Prediction

Introduction

In a manufacturing facility it is crucial to ensure tight tolerances using appropriate measuring instruments. This is a challenging task especially for the production of large-scale components, as the precise measurement of large structures can be very time-consuming. And it is still more demanding if the components will be employed in safety critical applications. To address this issue, we propose a wireless sensor network capable of measuring the surface shape and strain of an object in real-time during the manufacturing process. The paper presents a sensor network constructed with probes arranged in a grid on the object's surface, with interconnections similar to those used in a numerical Finite-Element-Method (FEM). The concept is illustrated in Fig. 1 for a small network. The necessary calculations for determining surface shape and strain from measurement data will be discussed. Each sensor probe determines the surface normal and distance to neighboring probes, allowing for accurate reconstruction of the surface shape and strain. Additionally, an uncertainty analysis is carried out for neighboring sensor pairs as well as for the complete network. The networks uncertainty will be estimated employing a simulation model.

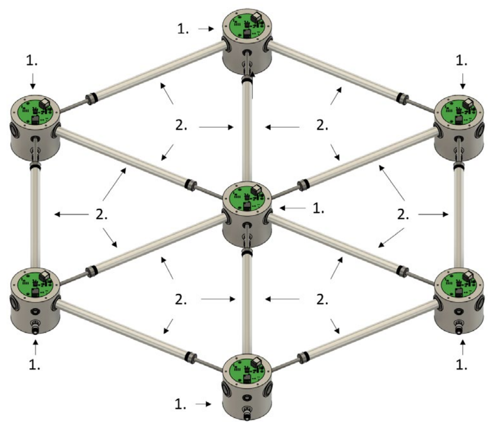

Fig. 1: Physical implementation of a FEM, 1. Sensor probe 2. Connecting rod.

DOI 10.5162/sensoren2024/D5.1

Sensor Network

The sensor network is composed of distributed wireless sensor probes that are interconnected through mechanical links to create a scalable network. Each sensor probe has its own local coordinate system, delivering information about the surface stress and deformation locally in the vicinity of the sensor probe evaluating the information's given by the sensors implemented in the probe and its direct neighbor probes. To determine the surface stress and deformation across the complete component the local information around each sensor probe has to be transformed into a global component coordinate system. The global component coordinate system is defined by reference probes with precisely determined positions S_{Ref}^{C} in the components coordinate system. In this notation the superscript indicates the coordinate system in which the position is calculated. Here, the superscript "*C*" denotes the global component coordinate system. In this sense the position of a sensor #j with respect to the local coordinate system of sensor #i is denoted by S_j^i. This is illustrated in Fig. 2. The position S_j^i is given in the local coordinate system of the probe #i and can be transformed into S_j^C transforming the position S_i^i into the global coordinate system. Thus, the position information of all the sensor probes in the global component coordinate system is the result of multiple transformations of positions given in a local coordinate system.

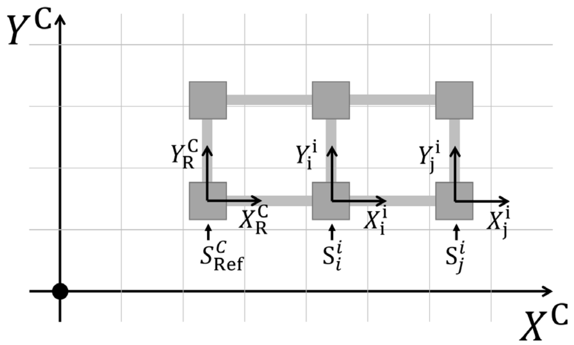

Fig. 2: Definition of the coordinate systems.

In order to determine the local position S_j^i each sensor probe determines the surface normal at its respective position using a 3D-inclinometer. Also, the mechanical links are equipped with an additional inclinometer to measure the inclination δ_{i-j} of the mechanical link. A linear variable differential transformer (LVDT) is used to measure the distance k_{i-j} between sensor probes. All inclinometers are realized by MEMS acceleration sensors. The mechanical connections are held in place with spherical ball bearings at each sensor probe. The position of all probes in the local coordinate system can be determined with the help of the measured angles and distances taking into account the geometric dependencies illustrated in Figure 3.

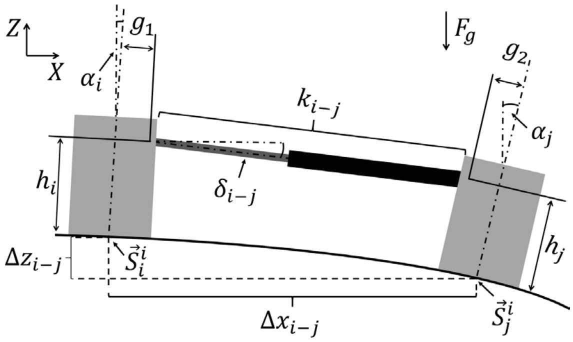

Fig. 3: Connection between two sensor probes with all necessary parameters and mechanical dimensions.

The angles δ_{i-j}, α_i and α_j need to be derived from the inclination sensor of the sensor probes and the connecting rod with respect to the Earths gravitational field $\vec{F}_g$. For 3D-position calculations the pitch ϕ and roll θ angle have to be calculated from the acceleration vector $\vec{a}_i$ to get the inclination angle α with

$$\phi_i = arctan\left(\frac{a_{i,x}}{a_{i,z}}\right), \tag{1}$$

$$\theta_i = \arctan\left(\frac{a_{i,y}}{\sqrt{a_{i,x}^2 + a_{i,z}^2}}\right). \tag{2}$$

Here, for the 2D case in Fig. 2 α is equal to the pitch angle ϕ, since there is only a rotation around the Y-axis. The inclination δ_{i-j} of the connecting rod is calculated from the measurement values given by the acceleration vector $\vec{a}_r$ from the sensor installed in the rod and the horizontal unity vector $\vec{e}_x$ in the X-axis direction via the scalar product relation according to

$$\delta_{i-j} = arccos\left(\frac{\vec{a}_r \cdot \vec{e}_x}{|\vec{a}_r| \cdot |\vec{e}_x|}\right) - \frac{\pi}{2}. \tag{3}$$

The angle δ_{i-j} is equal to $\frac{\pi}{2}$ in the case that the connecting rod is horizontal, therefore this offset must be subtracted to measure only the angle between the horizontal plane and the rod. The relative distances Δx_{i-j} and Δz_{i-j} from the left to the right probe are calculated via a vector addition of the vectors $\vec{p}_i$, $\vec{p}_i$ and $\vec{p}_{i-j}$ with the angles δ_{i-j}, α_i, α_j, the measured length k_{i-j}, the height h of the connecting rod to the object surface and the offset g to the center axis of the probe with

Tab. 1: Uncertainty contributions on the acceleration sensor

Standard uncertainty component	Source of uncertainty	Value of standard uncertainty $u(x_i)$	Probability distribution factor G_i	$c_i = \frac{\partial f}{\partial x_i}$	$u_i = \lvert c_i \rvert \cdot G_i \cdot u(x_i)$	Degrees of freedom ν_i
$u(a_{\mathrm{Cal}})$	Calibration uncertainty	1 mg	1	1	1 mg	1200
$u(a_{\mathrm{D}})$	Resolution ADC error	3.18 µg	$1/\sqrt{3}$	1	2.20 µg	∞
$u(a_{\mathrm{RMS}})$	Root-mean-square error	6.53 µg	1	1	6.53 µg	∞
$u(a_{\mathrm{T}})$	Temperature error	4 mg	$1/\sqrt{3}$	1	2.3 mg	∞
$u(a_{\mathrm{NL}})$	Nonlinearity error	4 mg	$1/\sqrt{3}$	1	2.3 mg	∞
					$U_a^2 = 11.67\ (\mathrm{mg})^2$ $U_a = 3.4$ mg $U_{a,95} = 6.8$ mg	> 1000

$$\vec{p}_i = h_i \cdot \begin{pmatrix} \sin(\alpha_i) \\ \cos(\alpha_i) \end{pmatrix} + gi \cdot \begin{pmatrix} \cos(\alpha_i) \\ -\sin(\alpha_i) \end{pmatrix}, \tag{4}$$

$$\vec{p}_j = h_j \cdot \begin{pmatrix} -\sin(\alpha_i) \\ -\cos(\alpha_i) \end{pmatrix} + g_i \cdot \begin{pmatrix} \cos(\alpha_i) \\ -\sin(\alpha_i) \end{pmatrix}, \tag{5}$$

$$\vec{p}_{i-j} = k_{i-j} \cdot \begin{pmatrix} \cos(\delta_{i-j}) \\ -\sin(\delta_{i-j}) \end{pmatrix}, \tag{6}$$

$$\vec{S}_j^i = \begin{pmatrix} \Delta x_{i-j} \\ \Delta y_{i-j} \end{pmatrix} = \vec{p}_i + \vec{p}_j + \vec{p}_{i-j}. \tag{7}$$

The vectors $\vec{p}_i$ and $\vec{p}_j$ represent the location of the rotation point of the bearing relative to the center of the sensor base. The orientation of the connecting rod in space is represented by the vector $\vec{p}_{i-j}$. In order to determine the global position of the second sensor probe, the local position of the right probe needs to be added to the global position of the probe $\vec{S}_i^C$ which can be expressed as

$$\vec{S}_j^C = \vec{S}_i^C + \vec{S}_j^i. \tag{8}$$

By using two or more reference probes with known positions on the component it is possible to determine the global positions of the probes along multiple paths, which can be averaged to minimize the uncertainty of each position. Additionally, with approach to evaluate multiple paths also offsets and calibration errors can be detected. It is assumed that changes in the surface strain or shape are spread over geometrical distances significantly larger than the distances between the individual sensor probes. Therefore, we made the distances between the sensor probes adjustable to meet the application requirements.

Uncertainty Estimation

The measurement uncertainty is estimated according to the “Guide of Uncertainty Measurement” [1]. The expanded uncertainty *U* in the position of a sensor probe can be expressed by the functional dependence $f(\vec{x})$ of the probe position with respect to the measured angels and distances included in the vector $\vec{x}$ and their individual standard uncertainties u_{x_n} according to

$$U = k \cdot \sqrt{\sum_{n=1} \frac{\partial f(\vec{x})}{\partial x_n} \cdot G_n \cdot u_{x_n}^2}. \tag{9}$$

With the weighting parameter G also non-Gaussian shaped probability density functions can be described, and the coverage factor k allows to consider different levels of confidence. The knowledge of the degrees of freedom are crucial as a normal distribution cannot be assumed for low degrees. For complex relationships the uncertainty estimation can be broken down in smaller subsystems, which then can be evaluated individually. Therefore, all of the used sensors in the network are evaluated first and this information was then combined to get an overall uncertainty estimation for all local connections, as is shown in Fig. 3. The curve describes the local position uncertainty of a specific sensor probe. In order to calculate the global position uncertainty of each probe, the local position uncertainties have to be brought into the global coordinate system using the information of the reference probes and the geometrical positions (paths) of the sensor probes within the network.

Uncertainty Estimation of the Angle Measurement

The accuracy of an angle measurement heavily depends on the uncertainty introduced by the acceleration sensor. We utilized the ADXL355 MEMS acceleration sensor from Analog Devices due to its built-in 20-bit internal analog-to-digital converter (ADC) and low noise performance [2]. All uncertainty contributions $u(\vec{x})$ on the three sensor axes and the expanded uncertainty of the accelerometer U_a for each axis are presented in Table I. The measurement values are expressed relative to the standard gravity in units of g. The position uncertainty of the acceleration sensor within the probe housing and zero offset of the accelerometer have a significant impact on the uncertainty, as is demonstrated in [3]. Therefore, it is necessary to calibrate the sensor properly using a suitable model. Additionally, the sensor axis must be aligned with the probe's coordinate system using a rotation matrix, which is also used to scale the accelerometer values. This allows for the sensor to be accurately modeled with

$$\begin{pmatrix} a_{\mathrm{x}}^{P} \\ a_{\mathrm{y}}^{P} \\ a_{\mathrm{z}}^{P} \end{pmatrix} = \begin{pmatrix} S_{\mathrm{x,x}} & S_{\mathrm{x,y}} & S_{\mathrm{x,z}} \\ S_{\mathrm{y,x}} & S_{\mathrm{y,y}} & S_{\mathrm{y,z}} \\ S_{\mathrm{z,x}} & S_{\mathrm{z,y}} & S_{\mathrm{z,z}} \end{pmatrix} \begin{pmatrix} a_{\mathrm{x}}^{S} \\ a_{\mathrm{y}}^{S} \\ a_{\mathrm{z}}^{S} \end{pmatrix} + \begin{pmatrix} b_{\mathrm{x}} \\ b_{\mathrm{y}} \\ b_{\mathrm{z}} \end{pmatrix}, \qquad (10)$$

$$\vec{a}^{P} = S \cdot \vec{a}^{S} + \vec{b}. \qquad (11)$$

The vector $\vec{a}^{P}$ represents the measurement data in the coordinate system of the sensor probe, which is transformed using the rotation matrix S from $\vec{a}^{S}$. The offset vector $\vec{b}$ is necessary to compensate static offsets in the sensor axis. In total the twelve parameters have to be determined employing a least-squares algorithm by rotating the sensor into predefined positions. Since the three accelerometer values $\vec{a}^{P}$ are independent of each other, each axis can be calculated individually [3]. The calibration quality can be determined according to [4] by comparing the actual accelerometer values, $\vec{a}^{P}$ with the measured values obtained through calibration $\vec{\hat{a}}^{P}$ with

$$\vec{u}^{2}(a_{\mathrm{Cal}}) = \frac{1}{N-1} \sum_{n=1}^{N} \left(\vec{a}^{P} - \vec{\hat{a}}^{P}\right)^{2}. \qquad (12)$$

The uncertainty $\vec{u}(a_{\mathrm{Cal}})$ describes the uncertainty of the sensor relative to the housing of the sensor probe with the variance of the fit residuals [4]. Based on this uncertainty, the uncertainties of the fit parameters can also be calculated according to [4], [5]. The used calibration uncertainty $\vec{u}(a_{\mathrm{Cal}})$ is determined through several calibrations evaluating different sensors, with 100 measurements taken for each rotation. Thus, the degrees of freedom for the calibration uncertainty is $\nu_{\mathrm{Cal}} = 1200$. Across all axes the uncertainty of the calibration is nearly the same with $u(a_{\mathrm{Cal}}) = 1\ \mathrm{mg}$. This uncertainty is used for the calculations in all axes. In this application it is also important to consider the temperature drift and nonlinearity of the sensor in order to ensure accurate measurements. We assume a maximum temperature drift of up to $10°\mathrm{C}$ in the operating environment. The sensor has a temperature sensitivity of $0.01\%/°\mathrm{C}$ of the full-scale measurement range and a nonlinearity of 0.1% [2]. A rectangular distribution is assumed for these parameters. Therefore, the standard uncertainty values are weighted with a factor $G_i = 1/\sqrt{3}$. The root-mean-square error of the sensors was determined by measuring over a time interval of approximately 24 hours using a third-order low-pass filter with a cut-off frequency of $1\ \mathrm{Hz}$ to further reduce sensor noise. The total standard uncertainty for each axis of the accelerometer is $U_{\mathrm{a}} = 3.4\ \mathrm{mg}$ with all contributions itemized in Tab. (1).

The uncertainty U_{ϕ} and U_{θ} is calculated from the uncertainties of the acceleration sensor using equations (1) and (2). Due to the nonlinearity of these formulas, uncertainties must be evaluated across the entire parameter space, resulting in a non-constant uncertainty for the ϕ uncertainty. This is due to a singularity in the angle determination when θ approaches $\pm 90°$, as shown in Fig. 3.

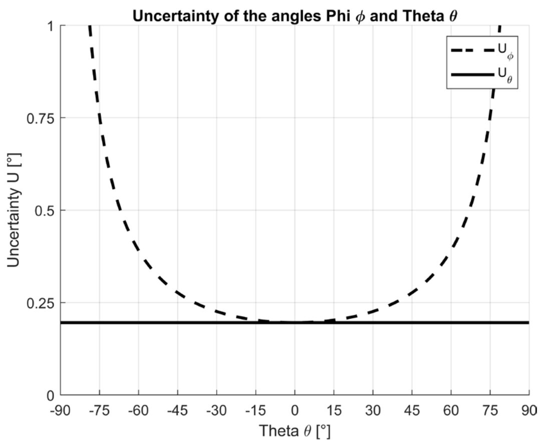

Fig. 3: Uncertainty of the angles ϕ and θ over the parameter space of θ.

This phenomenon is caused by the so-called gimbal lock effect, when describing rotations in 3D-space employing Euler angles. At these limits the uncertainty becomes infinite. Therefore, we limit the sensor's angle to the point where the uncertainty U_{ϕ} is smaller than $0.25°$. This means that the sensor may only rotate between ± 85 degrees using the ϕ angle. This restriction can only be met by avoiding to place sensor probes in an angle $\theta \approx \pm 90°$. The uncertainty of the angle θ stays constant over

DOI 10.5162/sensoren2024/D5.1

Tab.2: Uncertainty contributions on the length measurement

Standard uncertainty component	Source of uncertainty	Value of standard uncertainty $u(x_i)$	Probability distribution factor G_i	$c_i = \frac{\partial f}{\partial x_i}$	$u_i = \lvert c_i \rvert \cdot G_i \cdot u(x_i)$	Degrees of freedom ν
$u(k_\mathrm{D})$	Resolution ADC error	$50.4\ \mu\mathrm{V}$	$1/\sqrt{3}$	$1.7\ \mathrm{mm/V}$	$49.2\ \mathrm{nm}$	∞
$u(k_\mathrm{LVDT})$	LVDT sensor nonlinearity	$12.7\ \mu\mathrm{m}$	$1/\sqrt{3}$	1	$7.33\ \mu\mathrm{m}$	∞
$u(k_\mathrm{G})$	LVDT signal conditioner error	$18\ \mathrm{mV}$	$1/\sqrt{3}$	$1.7\ \mathrm{mm/V}$	$17.6\ \mu\mathrm{m}$	∞
$u(k_\mathrm{B})$	Bearing play	$32\ \mu\mathrm{m}$	$1/\sqrt{3}$	2	$36.9\ \mu\mathrm{m}$	∞
					$U_k^2 = 1.73\ (\mu\mathrm{m})^2$ $U_k = 41.6\ \mu\mathrm{m}$ $U_{k,95} = 83.2\ \mu\mathrm{m}$	∞

the complete parameter space. Thus, the θ angle can be measured with a higher confidence in all rotations of the probe. This is important to consider when mounting the sensor on a component surface with a strong curvature. For the connecting rod angle δ_{i-j}, the uncertainty can be calculated using Eq. (3). Due to the similar functional dependence of the input variables, it must be evaluated at each working point and is not constant over the entire parameter space of δ_{i-j}, as is shown in Fig.4. For this measurement the angle δ_{i-j} also needs to be limited to a maximum uncertainty of $0.5°$.

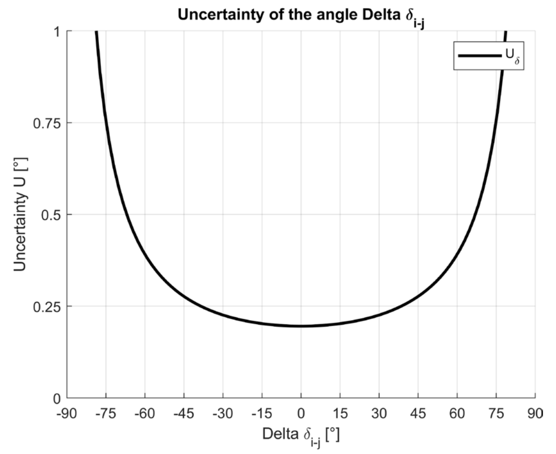

Fig. 4: Uncertainty of the angle delta over the parameter space of δ_{i-j}

The uncertainty of the angle measurement is rather big and can only be improved by reducing the uncertainty of the accelerometer sensor. This also showcases the limitations of angle measurements employing accelerometers.

Uncertainty Estimation of the Length Measurement

The first step to estimate the length or distance uncertainty is to determine the functional relationship with respect to the input parameters. As mentioned earlier, we used an LVDT sensor to measure the absolute distance between two probes. The LVDT sensor only measures the absolute distance over a small range, and therefore the nominal distance k_Nom needs to be added to determine the probes distance with

$$k_{i-j} = k_\mathrm{LVDT} + k_\mathrm{Nom}. \tag{13}$$

The distance measurement k_LVDT of the LVDT sensor is proportional to the sensors output voltage U_LVDT and can be expressed with

$$k_\mathrm{LVDT} = (d \cdot U_\mathrm{LVDT} + U_0). \tag{14}$$

The parameter d describes the gain factor between the distance and the sensor voltage output with a zero offset U_0. Thus, the distance k_{i-j} can be written in relation to the sensor voltage as

$$k_{i-j} = (d \cdot U_\mathrm{LVDT} + U_0) + k_\mathrm{Nom}. \tag{15}$$

The sensor has a nonlinearity of 0.25% for the full-scale range, which results in a nonlinearity uncertainty of $u(k_\mathrm{LVDT}) = 12.7\mu\mathrm{m}$. For a proper readout and condition of the sensor a special chip is used to operate the sensor, which also introduces uncertainty contributions to the measurement. In the datasheet of the chip a total error of 0.6% is given [6]. The output voltage of the chip is digitized with a 16-bit ADC, which adds a resolution error $u(k_\mathrm{D})$.The connecting rod is held in place at both ends with spherical ball bearings, which introduces play into the length measurement with a maximum play of $32\ \mu\mathrm{m}$ at each end [7]. Therefore, the bearing air contributes twice to the uncertainty estimate. All of the uncertainty sources and their contributions are presented in Tab. (2). Hence,

Tab.3: Uncertainty contributions on sensor probes position

Standard uncertainty component	Source of uncertainty	Value of standard uncertainty $u(x_i)$	Probability distribution factor G_i	$c_i = \frac{\partial f}{\partial x_i}$	$u_i = \|c_i\| \cdot G_i \cdot u(x_i)$	Degrees of freedom ν
$u(g)$	Manufacturing tolerance	$0.1\ \mathrm{mm}$	$1/\sqrt{3}$	c_g	u_g	∞
$u(h)$	Manufacturing tolerance	$0.1\ \mathrm{mm}$	$1/\sqrt{3}$	c_h	u_h	∞
$u(\alpha_i)$	Angle uncertainty	$u(\alpha_i(\phi_i,\theta_i))$	1	c_{α_i}	u_{α_i}	> 1000
$u(\alpha_j)$	Angle uncertainty	$u\left(\alpha_j(\phi_j,\theta_j)\right)$	1	c_{α_j}	u_{α_j}	> 1000
$u(\delta_{i-j})$	Angle uncertainty	$u(\delta_{i-j})$	1	$c_{\delta_{i-j}}$	$u_{\delta_{i-j}}$	∞
$u(k_{i-j})$	Distance uncertainty	$41.6\ \mu\mathrm{m}$	1	$c_{k_{i-j}}$	$u_{k_{i-j}}$	∞
$u(S_i)$	Position uncertainty	$u(S_i)$	1	c_{S_i}	u_{S_i}	∞

the functional relationship according to Eq. (15) is linear related to all of the uncertainty sources the uncertainty U_k is equal to $41.6\ \mu\mathrm{m}$ for the complete measuring range. Since all contributions have a degree of freedom going to infinity, the total degree of freedom is also infinite. For further improvement of the sensors uncertainty a calibration with a precision reference system should be done, like shown in [8].

Uncertainty Estimation of the Local Position

The uncertainty of the local position can be determined with the help of the previously determined sensor uncertainties and the mechanical uncertainties. Since the relative position of the sensor probe has three coordinates the uncertainty also has to be expressed in three dimensions. Therefore, the vector for the local position uncertainty $\vec{U}_j^i$ is given by

$$\vec{U}_j^i = \sqrt{\sum_{n=1}\left(\frac{\partial(\vec{S}_j^i)}{\partial \vec{x}_n}\cdot G_n \cdot \vec{u}_{x_n}\right)^2}. \qquad (16)$$

This position uncertainty is highly non-linear depending on the individual uncertainty components. In particular, the orientation of the surface normal has a strong effect on the position uncertainty due to the sine and cosine dependencies of the rotation angles, respectively. This is also important for the used uncertainties of the accelerometer sensors. Thus, the sensitivity coefficient and the sensor uncertainties have to be evaluated at each position. The mechanical uncertainties of the probe are given by the manufacturing tolerances, which are for both dimensions $\pm 0.1\ \mathrm{mm}$. All uncertainty contributions are displayed in Tab. (3). For the determination of the local position uncertainty the position uncertainty of $\vec{S}_i^i$ is assumed to be zero as sensor probe #*i* defines the origin of the local coordinate system. This results in a local uncertainty $\vec{U}_j^i$ of the probe that cannot be used to make statements about the position uncertainty $\vec{U}_j^C$ of the probe in the components coordinate system.

Sensor Network Uncertainty Estimation

In order to transfer the locally defined relative distance information of neighboring probes into the global component coordinate system reference probes are introduced. The uncertainty of a reference probe is given by the accuracy with which the reference probe can be positioned by a worker or robot in the component coordinate system. Thus, every non-referenced probe inherits the uncertainty of the reference probe $\vec{U}_{S_\mathrm{Ref}}$ and the uncertainties introduced by local connections to neighboring probes. Hence, the number of connections should be kept to a minimum, as the total uncertainty increases with the number of network nodes. The minimum number of “hops”, i.e. paths crossing a sensor probe, can be determined evaluating all possible paths between a reference sensor and a specific sensor probe. On each path the uncertainty propagates differently throughout the network. To reduce the position uncertainty the information of different paths can be fused [5],[9].

In order to showcase the uncertainty propagation through the network we simulated an example application, where 25 probes are arranged in a two-dimensional configuration on a semicircle with a diameter of six meters. By placing the sensor network on this semicircle, the sensor values are spread nearly over the

DOI 10.5162/sensoren2024/D5.1

complete parameter space. Two reference probes are placed on the left and right edge of the circular structure, which is shown in Fig. 5. Therefore, the position uncertainty of each of the non-referenced probes can be calculated on two different ways, with sensor #1 as reference of with sensor #25 as reference, respectively.

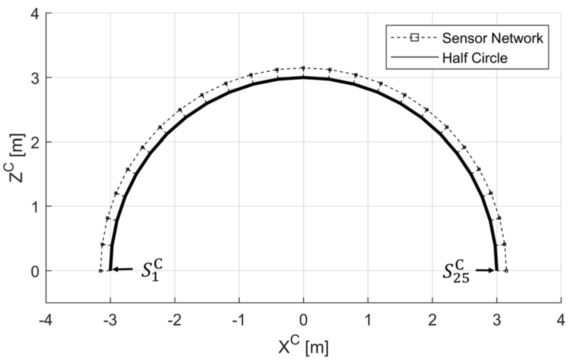

Fig. 5: Sensor network placed on a semicircle with two reference probes

The local and global position uncertainties of the sensor probes with respect to the left reference sensor #1 are shown in Figure 6. The position uncertainties with respect to reference sensor #25 behave similar and are only mirrored around sensor position S_{13}^C. For reference sensor #1 a position uncertainty of $0.1\mathrm{mm}$ is assumed. This is clearly recognizable in Fig. 6. As a result, all of the probes to the right cannot have a lower level of global uncertainty. As expected, probe #25, which is furthest away from reference sensor #1, has the highest position uncertainty of $2.8\ \mathrm{mm}$.

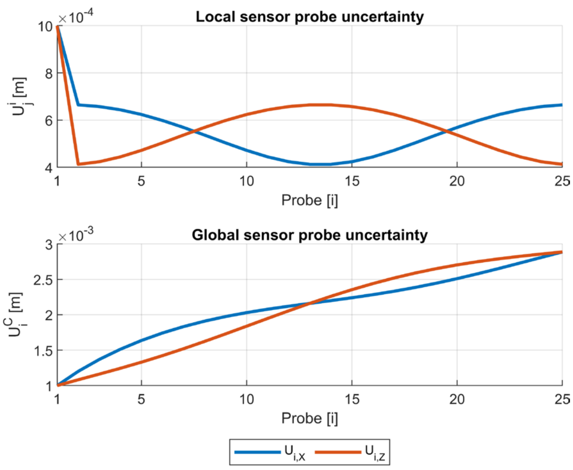

Fig. 6: Local and global sensor probe position uncertainties with respect to the left reference sensor #1.

Fig. 7 shows the result of the uncertainty calculations, where the position uncertainties of each sensor has been calculated as the weighted mean of two uncertainty estimations, the first one coming from the path originating from sensor #1 as reference and the second one coming from the path originating from sensor #25 as reference. As expected, the maximum position uncertainty exhibits sensor #13 with $1.52\ \mathrm{mm}$, lying in the middle between the reference probes. At the reference probes the uncertainty of the probes only decreases by a small amount when taking the second possible path into account.

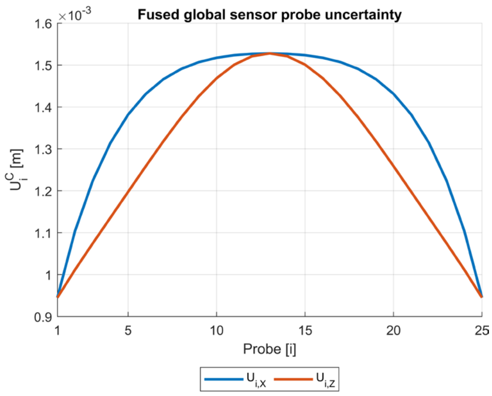

Fig. 7: Fused global sensor probe uncertainty from the left and right reference

Conclusion

This paper presents the construction and calculations for a wireless sensor network for the determination of shape and surface stress of large objects. Additionally, we evaluated the uncertainties of the complete sensor network by individually assessing each sensor (network node), considering their individual uncertainties. This highlights the challenges of estimating uncertainties with nonlinear relations. Combining all uncertainty quantities allows for the estimation of both local and global position uncertainties of the sensor probes. Global uncertainty propagates through the network and increases with every additional connection. However, position uncertainty can be reduced by fusing different paths originating from multiple reference probes. In a future work, the sensor uncertainties will be further reduced to improve the overall accuracy of the sensor network.

Acknowledgements

The authors would like to acknowledge Mrs. Katharina Sophie Isleif and Mr. Jonas Jockram for their highly appreciable continuous support.

This work is a part of the “Digital Sensor-2-Cloud Campus Platform” (DS2CCP) project, which is funded by the Federal Ministry of

Defense under the dtec.bw program. Project website:
https://dtecbw.de/home/forschung/hsu/projekt-ds2ccp/projekt-ds2ccp

References

[1] BIPM *et al.*, "Evaluation of measurement data — Guide to the expression of uncertainty in measurement." Joint Committee for Guides in Metrology, JCGM 100:2008. [Online]. Available: https://www.bipm.org/documents/20126/2071204/JCGM_100_2008_E.pdf/cb0ef43f-baa5-11cf-3f85-4dcd86f77bd6

[2] Analog Devices Inc., *ADXL354/ADXL355*, Rev. A. 2018. Accessed: Dec. 22, 2023. [Online]. Available: https://www.analog.com/media/en/technical-documentation/data-sheets/adxl354_355.pdf

[3] Z. Chen, H. Li, X. Du, and J. Yan, "Research on the Calibration Method of MEMS Accelerometer Based on Recursive Least Squares," in *2018 IEEE International Conference on Mechatronics and Automation (ICMA)*, Aug. 2018, pp. 533–538. doi: 10.1109/ICMA.2018.8484627.

[4] W. Ilewicz, K. Skrzypczyk, A. Galuszka, T. Grzejszczak, D. Bereska, and M. Pacholczyk, "Estimation of Uncertainty of IMU Module Measurement Results," in *2018 International Conference on Signals and Electronic Systems (ICSES)*, Sep. 2018, pp. 92–95. doi: 10.1109/ICSES.2018.8507321.

[5] M. Gruber *et al.*, "Application of Uncertainty-Aware Sensor Fusion in Physical Sensor Networks," in *2022 IEEE International Instrumentation and Measurement Technology Conference (I2MTC)*, May 2022, pp. 1–6. doi: 10.1109/I2MTC48687.2022.9806580.

[6] Analog Devices Inc., *AD598*, Rev. A. Accessed: Dec. 22, 2023. [Online]. Available: https://www.analog.com/media/en/technical-documentation/data-sheets/ad598.pdf

[7] Schaeffler Technologies AG & Co. KG, *Plain Bearings*. Accessed: Dec. 22, 2023. [Online]. Available: https://www.schaeffler.com/remotemedien/media/_shared_media/08_media_library/01_publications/schaeffler_2/catalogue_1/downloads_6/hg_1_de_en.pdf

[8] V. Tudic, "Uncertainty evaluation of slope coefficient of high precision displacement sensor," in *Proceedings ELMAR 2006*, Jun. 2006, pp. 231–234. doi: 10.1109/ELMAR.2006.329555.

[9] R. Wang and S. Sun, "Distributed Matrix-Weighted Fusion Consensus Filtering With Two-Stage Filtering for Sensor Networks," *IEEE Sens. J.*, vol. 23, no. 5, pp. 5003–5013, Mar. 2023, doi: 10.1109/JSEN.2023.3235996.